Neural Network as a Cost Function for EPSO Algorithm in Perovskite Solar Cell Simulation

Daniyal Khosh Maram
Department of Electrical Engineering,
Amirkabir University of Technology
Tehran, Iran
Danialkhoshmaram@aut.ac.ir

Abstract

Time-consuming is one of the main bottlenecks in the SCAPS-1D simulations in the case of more computational data set. In this regard, we are achieving outputs data in SCAPS-1D and repeat this simulation by employing a neural network as a cost or target function for the evolutionary particle swarm optimization (EPSO) algorithm to decrease the computational expensiveness of SCAPS-1D simulation. Optimization and numerical simulation tools pave the way for having a better insight into the designing of perovskite solar cells. Also, it allows finding a relation between artificial intelligence and device physics.

Index Terms

Perovskite solar cell, neural network, optimization, evolutionary particle swarm optimization (EPSO), SCAPS-1D, artificial intelligence, device physics.

I. Introduction

Based on statistics, energy consumption had increased by around 100% from 1972 to 2004 [1]. To preventing further irreversible damage, it is essential to look for clean, diverse, and affordable energy solutions. One of the most promising candidates for renewable energy is solar energy because of a more cost-effective solution with faster installation and more predictive energy outputs [2]. Solar energy is one of the green clean energy sources with a wide range of applications. Perovskite solar cells (PSCs) caught great attention because of their remarkable rapid growth, possessing satisfying stability, low cost, and a simple fabrication process of PCE in the photovoltaic industry [3]–[5]. At first, the efficiency of PSCs was around 3.8% but recently increased enormously to a record to 24.2% in single-junction perovskite solar cells [6] and 25.2% in the perovskite/silicon tandem solar cells [7]. High carrier mobility, fitting bandgap, and long diffusion length are promising properties of perovskite materials. [8]–[11].

II. Perovskite solar cell Structure

The typical structure of PSCs consisting of a perovskite layer as an absorber sandwiched between two layers as an electron transfer layer (ETL) and hole transfer layer (HTL). In the typical structure of PSCs, the conduction band in the HTL must be above that in the perovskite, and the valence band in the ETL must be below that in the perovskite and According to this materials are chosen [12]. In the perovskite structure for leading holes and electrons towards HTL and ETL respectively, could be employed a generated built-in electric field arising from the discrepancies in the band energies of the different layers, and these make a potential barrier that exists to the entry of electrons into HTL and holes into ETL from perovskite [13]. Generally, methylammonium lead tri-iodide ($CH_3NH_3PbI_3$) is using as a perovskite absorbing material in PSCs [14]. According to [15], [16], $CH_3NH_3SnI_3$ has a narrower bandgap (1.3[eV]) than $CH_3NH_3PbI_3$.in which it can increase the electric field inside the semiconductor region [17], leading to the carrier generation rate in solar cells. According to [18], the PCE of $CH_3NH_3PbI_3$ PSC consisting of $CH_3NH_3SnI_3$ layer, increased from 14.32% to 15.32%. In this work, we present a PSC simulation based on the SCAPS-1D. We are employing PCBM as ETL and Cu_2O as HTL, and a layer of the $CH_3NH_3SnI_3$ is added between PCBM and $CH_3NH_3PbI_3$ layers, as shown in Fig. 1. The simulation parameters of PSC structure are shown in Table I [11], [18] and there are seven variable inputs series for neural network in up to 3000 iteration for sweep parameters, including the thickness of $CH_3NH_3SnI_3$, $CH_3NH_3PbI_3$, PCBM, Cu_2O, the bandgap of $CH_3NH_3SnI_3$, and $CH_3NH_3PbI_3$ and hole mobility of Cu_2O.and there are four outputs including V_{oc}, J_{sc}, FF, eta. One of the main bottlenecks in the simulation is that obtaining outputs is very time-consuming. Based on the structure mentioned earlier, we were swiping our inputs data to achieving outputs data in SCAPS-1D to repeat this simulation by employing neural network for decreasing the computational expensiveness of SCAPS-1D simulation. the main issue with this simulation based on neural networks

TABLE I
Simulation Parameters of the structure.

Material Quantity	PCBM	$CH_3NH_3PbI_3$	$CH_3NH_3SnI_3$	Cu_2O
Bandgap (eV)	2	1.55	1.3	2.24
Electron mobility ($cm^2/V.s$)	2×10^{-1}	10	1.6	30
Hole mobility ($cm^2/V.s$)	2×10^{-1}	10	1.6	30
Acceptor concentration ($1/cm^3$)	0	10^{+9}	$3 \times 10^{+16}$	$1.5 \times 10^{+15}$
Donor concentration ($1/cm^3$)	$2.93 \times 10^{+17}$	10^{+9}	0	0
Dielectric permittivity	3	10	8.2	7.5
Conduction Band DOS ($1/cm^3$)	$2.5 \times 10^{+21}$	$2.5 \times 10^{+20}$	10^{+18}	10^{+19}
Valence Band DOS($1/cm^3$)	$2.5 \times 10^{+21}$	$2.5 \times 10^{+20}$	10^{+18}	10^{+19}
Electron affinity (eV)	3.9	3.9	4.17	3.4

is that this technique is reliable just in the structure that mentioned it earlier. However, it is undeniable that the approach and provided code is flexible to calculate expected values in any perovskite solar cell structure in further study.

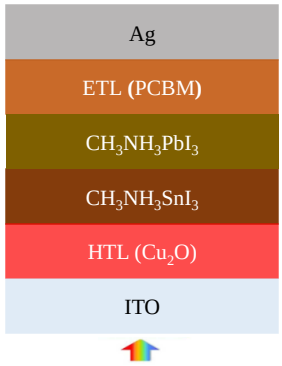

Fig. 1: Device structure cartoon.

III. Optimization Results

In this work, we utilized a neural network with two hidden layers so that the first hidden layer has nineteen neurons, and the second layer has five neurons. Evolutionary Particle Swarm Optimization (EPSO) algorithm employed for the training of this neural network [19]. In here to prediction outputs, there are four neural networks for every four outputs. Inside of these layers, there is one neuron with a linear activation function. All data becoming to 3 parts, so that first part includes train data around 70% of all data, and the second part includes test data around 15% of all data, and the third part comprises validation data around 15% of all data to tuning hyperparameters. For loss function, the Mean squared error (MSE) function utilized. Initial weights have been initialized Randomly. For the regression problems, a factor defined R^2 has been utilized typically. The value of R^2 would be between 0 and 1; if this value was closest to one, it means the network is trained right and yields a better fit for data. if the R^2 factor of the train is much more than the R^2 factor of the test means the neural network is overfitting on the training. Overfitting is the case where the overall cost is really small, but the generalization of the model is unreliable. This is due to the model learning "too much" from the training data set. if the R^2 factor of the train is closest to 0.5 means, the neural network is underfitting on the inputs. Underfitting is the case where the model has "not learned enough" from the training data, resulting in low generalization and unreliable predictions. If R^2 value was closest to one, it means the network is trained right and yields a better fit for data. In Fig. 2, Fig. 4, Fig. 6, and Fig. 8 that the R^2 factor of the train is much more than the R^2 factor of the test means the neural network is overfitting on the training. In Fig. 3,

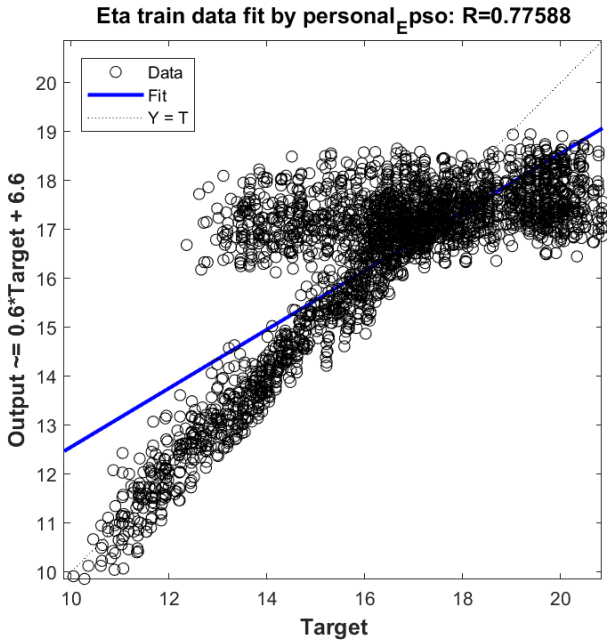

Fig. 2: Plotregression of train data of eta vs fit.

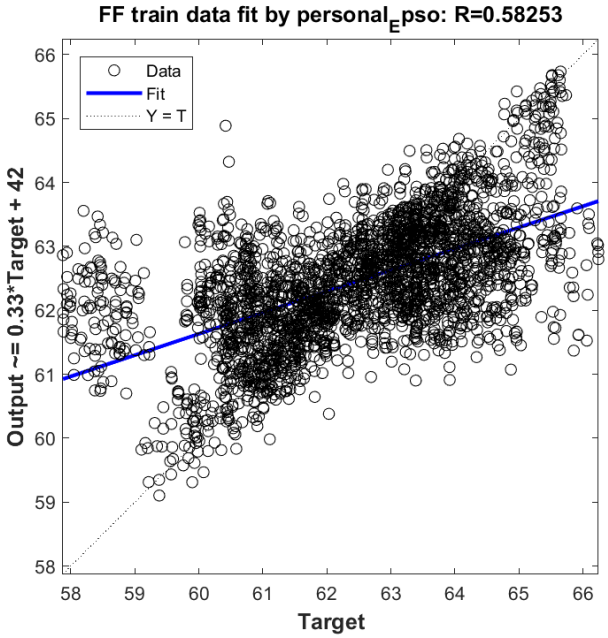

Fig. 3: Plotregression of train data of FF vs fit.

Fig. 5, Fig. 7, and Fig. 9 that the R^2 factor of the train is closest to 0.5 means, the neural network is underfitting on the inputs.

IV. Conclusion

In this work, we employed a structure mentioned earlier. One of the main bottlenecks in the simulation is that obtaining outputs is very time-consuming in the terms of more sweep data. The main issue with this simulation based on neural networks is that this technique is reliable just in the structure that mentioned it earlier. We repeat this simulation by employing neural network as a cost function for optimization via EPSO for decreasing the computational expensiveness of SCAPS-1D simulation and further calculation accuracy. The future works could be extending this work to a neural network with more data set and expanding to more different structures for PSCs.

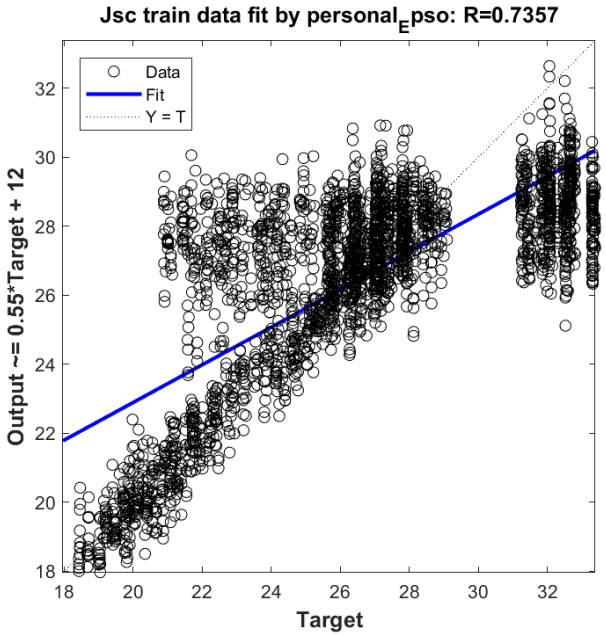

Fig. 4: Plotregression of train data of J_{sc} vs fit.

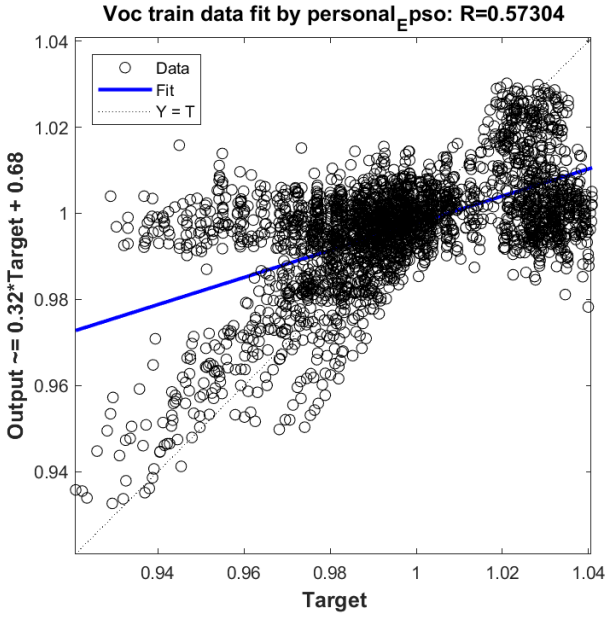

Fig. 5: Plotregression of train data of V_{oc} vs fit.

V. Acknowledgement

The authors would like to acknowledge Dr. Marc Burgelman from University of Gent for providing SCAPS simulation software and its free access.

VI. Conflict of Interest

There is no conflict of interest.

References

[1] T. Stocker, Climate change 2013: the physical science basis: Working Group I contribution to the Fifth assessment report of the Intergovernmental Panel on Climate Change. Cambridge University Press, 2014.
[2] NASA, Nasa - clean energy,. NASA, 2016.

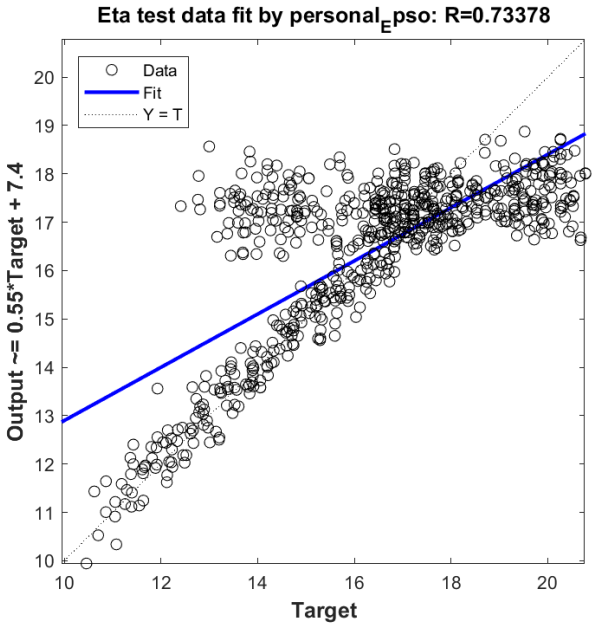

Fig. 6: Plotregression of test data of eta vs fit.

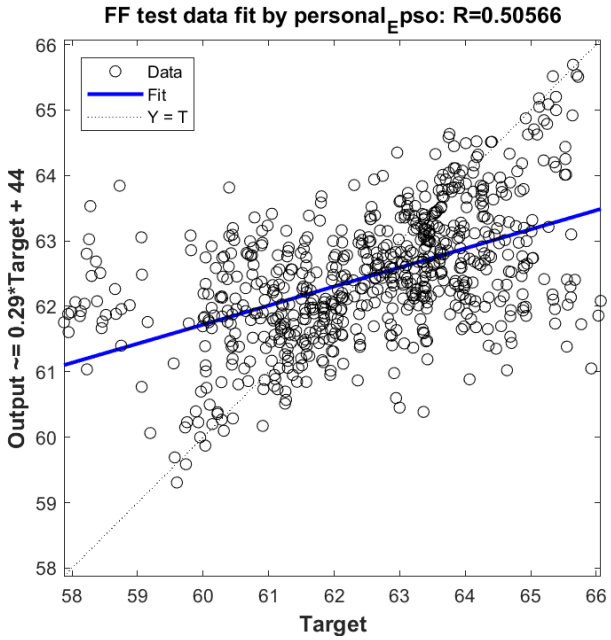

Fig. 7: Plotregression of test data of FF vs fit.

[3] G.-X. Liang, P. Fan, D. Gu, Z.-H. Zheng, D.-P. Zhang, J.-T. Luo, X.-H. Zhang, and H.-L. Ma, "Enhanced crystallinity and performance of ch3nh3pbi3 thin film prepared by controlling hot ch3nh3i solution onto evaporated pbi2 nanocrystal," IEEE Journal of Photovoltaics, vol. 6, no. 6, pp. 1537–1541, 2016.
[4] D. Shi, V. Adinolfi, R. Comin, M. Yuan, E. Alarousu, A. Buin, Y. Chen, S. Hoogland, A. Rothenberger, K. Katsiev, et al., "Low trap-state density and long carrier diffusion in organolead trihalide perovskite single crystals," Science, vol. 347, no. 6221, pp. 519–522, 2015.
[5] S. Pisoni, R. Carron, T. Moser, T. Feurer, F. Fu, S. Nishiwaki, A. N. Tiwari, and S. Buecheler, "Tailored lead iodide growth for efficient flexible perovskite solar cells and thin-film tandem devices," NPG Asia Materials, vol. 10, no. 11, p. 1076, 2018.
[6] NREL, NREL Efficiency chart. NREL, 2019.
[7] F. Sahli, J. Werner, B. A. Kamino, M. Bräuninger, R. Monnard, B. Paviet-Salomon, L. Barraud, L. Ding, J. J. D. Leon, D. Sacchetto, et al., "Fully textured monolithic perovskite/silicon tandem solar cells with 25.2% power conversion efficiency," Nature materials, vol. 17, no. 9, p. 820, 2018.
[8] P. Gao, M. Grätzel, and M. K. Nazeeruddin, "Organohalide lead perovskites for photovoltaic applications," Energy & Environmental Science, vol. 7, no. 8, pp. 2448–2463, 2014.
[9] P. P. Boix, K. Nonomura, N. Mathews, and S. G. Mhaisalkar, "Current progress and future perspectives for organic/inorganic perovskite

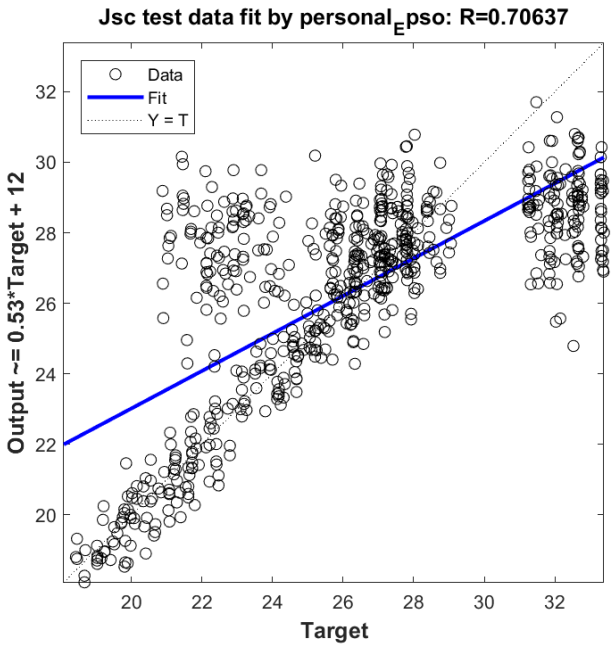

Fig. 8: Plotregression of test data of J_{sc} vs fit.

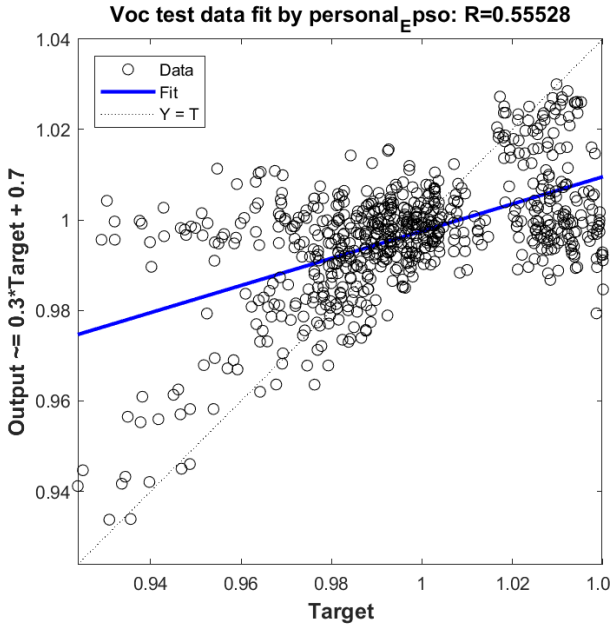

Fig. 9: Plotregression of test data of V_{oc} vs fit.

solar cells," Materials today, vol. 17, no. 1, pp. 16–23, 2014.

[10] K. Tanaka, T. Takahashi, T. Ban, T. Kondo, K. Uchida, and N. Miura, "Comparative study on the excitons in lead-halide-based perovskite-type crystals ch3nh3pbbr3 ch3nh3pbi3," Solid state communications, vol. 127, no. 9-10, pp. 619–623, 2003.

[11] D. K. Maram, H. Habibiyan, H. Ghafoorifard, and O. Shekoofa, "Analysis of optimum copper oxide hole transporting layer for perovskite solar cells," in 2019 27th Iranian Conference on Electrical Engineering (ICEE), pp. 214–219, April 2019.

[12] E. L. Unger, E. T. Hoke, C. D. Bailie, W. H. Nguyen, A. R. Bowring, T. Heumüller, M. G. Christoforo, and M. D. McGehee, "Hysteresis and transient behavior in current–voltage measurements of hybrid-perovskite absorber solar cells," Energy & Environmental Science, vol. 7, no. 11, pp. 3690–3698, 2014.

[13] H. J. Snaith, A. Abate, J. M. Ball, G. E. Eperon, T. Leijtens, N. K. Noel, S. D. Stranks, J. T.-W. Wang, K. Wojciechowski, and W. Zhang, "Anomalous hysteresis in perovskite solar cells," J. Phys. Chem. Lett, vol. 5, no. 9, pp. 1511–1515, 2014.

[14] T. J. Jacobsson, J.-P. Correa-Baena, M. Pazoki, M. Saliba, K. Schenk, M. Grätzel, and A. Hagfeldt, "Exploration of the compositional space for mixed lead halogen perovskites for high efficiency solar cells," Energy & Environmental Science, vol. 9, no. 5, pp. 1706–1724, 2016.

[15] C. C. Stoumpos, C. D. Malliakas, and M. G. Kanatzidis, "Semiconducting tin and lead iodide perovskites with organic cations: phase transitions, high mobilities, and near-infrared photoluminescent properties," Inorganic chemistry, vol. 52, no. 15, pp. 9019–9038, 2013.

[16] P. Umari, E. Mosconi, and F. De Angelis, "Relativistic gw calculations on ch 3 nh 3 pbi 3 and ch 3 nh 3 sni 3 perovskites for solar cell applications," Scientific reports, vol. 4, p. 4467, 2014.
[17] T. H. Anderson, M. Faryad, T. G. Mackay, A. Lakhtakia, and R. Singh, "Combined optical–electrical finite-element simulations of thin-film solar cells with homogeneous and nonhomogeneous intrinsic layers," Journal of Photonics for Energy, vol. 6, no. 2, p. 025502, 2016.
[18] S. Zandi and M. Razaghi, "Finite element simulation of perovskite solar cell: A study on efficiency improvement based on structural and material modification," Solar Energy, vol. 179, pp. 298–306, 2019.
[19] A. Lorestani and S. H. H.-M. M. Ardehali, "An evolutionary particle swarm optimization for multi-objective optimal reactive power planning considering voltage stability, voltage deviation and investment cost of tcsc,"